Cement & Concrete Composites 33 (2011) 867–880

Contents lists available at ScienceDirect

Cement & Concrete Composites

journal homepage: www.elsevier.com/locate/cemconcomp

Damage distribution and size effect in numerical concrete from lattice analyses

H.-K. Man, J.G.M. van Mier *

ETH Zurich, Institute for Building Materials, 8093 Zurich, Switzerland

ARTICLE INFO

Article history:
Received 30 September 2010
Received in revised form 25 January 2011
Accepted 27 January 2011
Available online 3 February 2011

Keywords:
Numerical concrete
Lattice model
Aggregate density
Aggregate shape
Crack size distribution
Size effect
Weibull model

ABSTRACT

Size effect on structural strength of concrete prisms subjected to three-point bending has been studied using the lattice model, which has been extended and now contains a realistic aggregate structure of concrete. The aggregate structure was obtained from CT-scans of real concrete prisms and overlaying the obtained image with a 3-dimensional hcp-lattice. The numerical analyses show that a size effect on structural strength exists for all studied aggregate densities and aggregate shapes. The size effect can be approximated with a Weibull model, where the main parameter, the Weibull modulus, depends on the concrete composition. The crack size distributions have been calculated and show a similar distribution as hypothesized before for fracture in ceramics. The results from the crack size distribution are helping to provide insight into the nature of the fracture process, which seems to differ from that hitherto assumed in cohesive crack models. After a weakening of the material through a multitude of microcracks, at peak load a single large crack propagates while loading continues in the softening regime. The presumed 'cloud of microcracks' advancing ahead of the macro-crack tip has not been found. Instead an alternative macroscopic model strategy, referred to as the 4-stage fracture model, is proposed.

1. Introduction

For many years it is known that structural strength varies with size. Leonardo da Vinci and Galileo Galilei are often recognised as pioneers studying the size effect on structural strength. For many materials a decrease of structural strength is observed with increasing size. The normal way of plotting data is in a log (nominal strength) versus log (characteristic size) diagram, as can be seen in the bulk of the literature dealing with size effect and scaling, e.g. Walsh [1], Bažant [2] and Carpinteri et al. [3]. Structural disasters like the collapse of the Koror Babelthuap Bridge in Palau in 1996 are attributed, at least to some extent, to our failing knowledge of structural behaviour at those large sizes (Burgoyne and Scantlebury [4]), where it should be added that in the example not all conditions at the time of the collapse were known, and perhaps a simple and straightforward explanation can be given other than size effect.

Laboratory experiments on concrete and concrete structures are almost per definition at small scale. Ease of handling is one of the main reasons to test small-sized samples; on top of that also the costs of the experiments may play a role. In [5] most of the available data for shear failure in reinforced concrete beams are shown in a log σ_N–log D plot, which shows a clear lower bound of specimen/beam sizes of 100 mm, whereas the largest tested samples do not exceed 20 m. Perhaps one of the largest beams ever tested is 36-m long beam used for studying the behaviour of reinforced concrete in shear [6]. The largest structures ever tested in the field of geo-materials are probably the floating ice sheet tests by Dempsey et al. [7,8]. In Fig. 1 the range of the majority of experimental data is shown together with some of the current theories. The experimental range is small, considering that the largest span in the Koror Babelthuap Bridge was about 240 m. The size range of interest actually lies just beyond the current experimental range of laboratory experiments. The following two questions are considered most important:

(1) What is the physical reason for the decrease of strength for larger sizes? and,
(2) How should information obtained for small structural sizes (in the laboratory) be extrapolated to real full-scale structural sizes?

The first to address question (1) in modern times was Weibull [9,10], who asserted that larger structures have a larger chance of containing a critical flaw that may lead to complete collapse. This approach, the so-called weakest link method, has its basis in statistics. In addition to the weakest link hypothesis, it is assumed that the structure will fail as soon as the first critical defect fails. In the double logarithmic plot of Fig. 1, the Weibull theory is represented by a straight line; the negative power is the result of several parameters, namely the dimensionality of the problem (typical 2D or 3D problems are considered with $n = 2$ and 3 respectively), and the so-called Weibull modulus m, which is considered a material

* Corresponding author.
E-mail addresses: jvanmier@ethz.ch, jvanmier@xs4all.nl (J.G.M. van Mier).

0958-9465/$ - see front matter © 2011 Elsevier Ltd. All rights reserved.
doi:10.1016/j.cemconcomp.2011.01.008

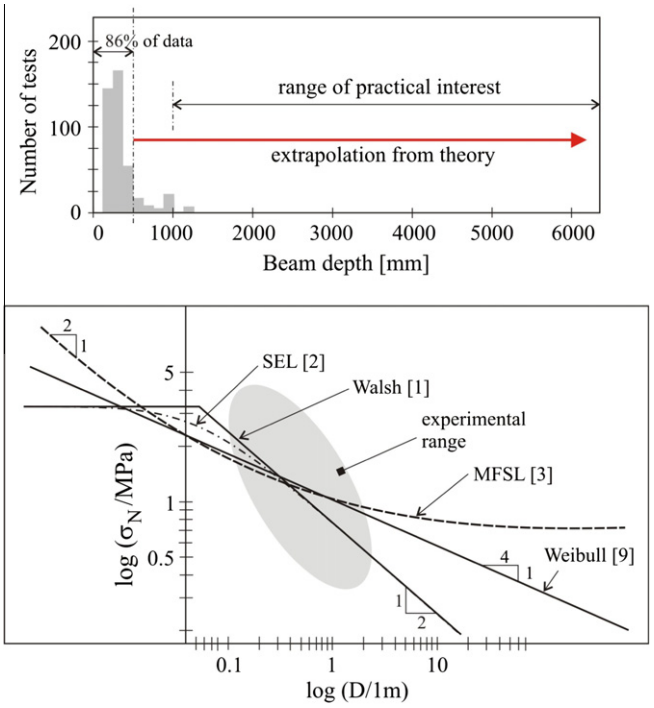

Fig. 1. Log σ_N–log D plot showing the decrease of nominal strength for structures with varying size, from [5]. The range of available experimental data lies between 100 mm and 2000 mm beam depth. Different models have been developed in the past, notable the Weibull power law [9,10], the size effect law [2] and the multifractal scaling law [3,12]. Walsh's [1] original work has also been included. Note that Walsh's results indicate a LEFM slope of −1/2 for large beam sizes; the same asymptotic value has later been used in [2]. The key questions are twofold: understanding why strength varies with structural size, and how information from small size experiments should be extrapolated to practical sizes.

property. The nominal strength can be shown to depend on structural size following [11]:

$$\sigma_N \propto D^{-n/m}. \tag{1}$$

When the reason for the decrease of strength is known, extrapolating the results to larger sizes will follow in a simple and straightforward manner. It seems therefore that the first question always must precede the second one.

Currently, in engineering, there are two schools debating their approaches for explaining size effect on structural strength and fracture energy. The first approach is based on a so-called statistical-energetic hypothesis [2], whereas the second method is based on considerations of the fractal geometry of the microcrack structure at peak stress, [3,12]. Both approaches are phenomenological.

In addition to the debate between engineers, there is a third school that addresses the role of disorder in quasi-brittle materials by means of methods derived from statistical physics. Lattice-type models are quite useful in this respect because of their inherent simplicity. Fuse lattices as an equivalent to more demanding central force and beam lattices, with or without quenched or annealed disorder are used (see for example [13,14]), and lattices with superimposed computer-generated structure of the considered material in 2- or 3-dimensions (for example [15–18]). Based on these latter approaches, other models were developed, e.g. [19,20] and many others. More recent is the use of realistic material structures, [21–23]. The obvious advantage of lattice models is their simplicity: (1) the fracture law can be a purely elastic-brittle law as an approximation of the more complicated fracture potential that appears at various levels of observation [24], and (2) the real structure of the material can be included directly in the models, which allows to study fracture mechanisms and size effects on fracture in the same way as in the laboratory, without premature assumptions on asymptotic behaviour as is required in phenomenological engineering models such as [2]. The obvious disadvantage is the large computational effort, where however the situation is gradually improving with advances in computer technology. Here the view of Emery et al. [25] is shared: available computer facilities should be used to our advantage as much as possible. The tools are excellent, especially when used in a sensible way in combination with experiments.

In this paper we will first give an overview of the Weibull method, an empirical method, which relies on knowledge of an exponent m, referred to as the Weibull modulus as mentioned above (Eq. (1)). In the original approach the Weibull modulus was determined from experiments, but recently, efforts have been made to give this important parameter a more theoretical footing. In Section 3 the lattice model, which we have used since 1990 for the study of fracture processes in (numerical) concrete, will be presented. Analyses of prisms of different sizes, loaded in three-point bending, shed some light on the physical reasons behind the size effect on strength and load–displacement behaviour. In our lattice model realistic material structures are currently incorporated, measured in the laboratory by means of X-ray (CT) scans of concrete containing varying amounts of aggregates of varying shape. This extension has been made in the doctoral thesis of the first author. Of particular importance is the analysis of the 'crack size distribution' or 'damage distribution' in the prisms not only at peak load, but during the entire loading history to complete rupture. These results are presented in Section 4. All the analyses carried out are in full 3D, which is in contrast to most phenomenological approaches, e.g. [2], where for convenience the third dimension was omitted and structures of the same thickness were studied. In Sections 5 and 6 we discuss our results in a wider context, present the conclusions, and end by indicating future directions for research.

2. Weibull methodology

The strength of brittle materials is commonly described by means of the statistical method devised by Weibull [9,10]. Weibull developed an empirical formula that describes the variation in the strength of materials based on the so-called weakest-link concept. The probability for failure P_f depends on stress σ and is given by

$$P_f(\sigma, V) = 1 - \exp\left\{-\frac{V}{V_0}\left(\frac{\sigma}{\sigma_0}\right)^m\right\}, \tag{2}$$

where m is the so-called Weibull modulus, which must be determined experimentally, V is the volume of the considered material, V_0 is the chosen normalising volume and σ_0 is a normalising stress (characteristic strength). Often a lower limit for the strength σ_u is included, with a probability for failure equal to zero:

$$P_f = 1 - \exp\left\{-\frac{V}{V_0}\left(\frac{\sigma - \sigma_u}{\sigma_0}\right)^m\right\}. \tag{3}$$

The strength of a material/structure depends on the actual damage or microcrack distribution at the moment just before failure; see for example Jayatilaka and Trustum [26] and Danzer et al. [27]. Jayatilaka and Trustum give a probability density $f(a)$ of semi-crack length a ($a \geqslant 0$) as follows:

$$f(a) = \frac{c^{n-1}}{(n-2)!}a^{-n}e^{-c/a}, \tag{4}$$

where c is a scaling parameter and n determines the length of the tail of the density function. The larger flaw sizes in the tail of the probability density $f(a)$ most likely control the strength of the

material. There the largest flaws are found, which tend to be more critical. The question to be posed is of course whether this idea can be applied to materials like concrete and rock (like limestone, granite) where heterogeneity plays a large(r) role. Cracks can be arrested in the heterogeneous material structure, and perhaps it is more likely that the details of the microstructure need to be included in any formulation.

Jayatilaka and Trustum continue to include fundamentals of linear elastic fracture mechanics and finally relate the probability of failure for a single crack by means of

$$F(\sigma) = \int_{\kappa}^{\infty} \left[1 - \frac{\kappa}{a}\right] \frac{c^{n-1} a^{-n} e^{-c/a}}{(n-2)!}\, da, \tag{5}$$

with $\kappa = K_{Ic}^2/(\pi\sigma^2)$. Only a crack of sufficiently large size a will lead to failure, since one may expect that the critical stress intensity is reached earlier than for other cracks in the population. In the above it is assumed that any crack orientation is equally likely. From Eq. (5) it is then possible to compute the probability of failure for different values of σ, where one should consider the effect of N defects (crack) in the material sample. Similar derivations are given in [27], where the fracture probabilities of ceramics are analyzed. It is assumed that damage is sparsely distributed with a relative frequency following an inverse power law as shown in Fig. 2:

$$g(a) = g_0 \left(\frac{a}{a_0}\right)^{-r}, \tag{6}$$

The relative flaw density derived is equal to

$$g(a) = \frac{m}{2V_0} \left(\frac{K_{Ic}}{Y\sigma_0\sqrt{\pi}}\right) a^{-n}, \tag{7}$$

where $m = 2n - 2$, and Y is the geometrical factor as defined in classical LEFM. The shape of the defect size distribution $f(a)$ or $g(a)$ is of importance. It is not so much the distribution at small crack length, but rather the tail of the diagram that seems to determine the strength of materials. Note that the critical defect size a_c decreases with increasing stress-level σ. Thus the shaded area in Fig. 2 gradually becomes larger with increasing stress, meaning that the mean number of destructive flaws increases.

Danzer et al. [27] show that for ceramics with sparsely distributed defects the probability of failure can be described by means of a Weibull distribution with $m = 15$.

For (numerical) concrete, the damage distribution can now be calculated. This has been done in the present paper for concrete with different aggregate shapes and different aggregate densities. Some preliminary results have been obtained in the past [17]; here we show more extensive results.

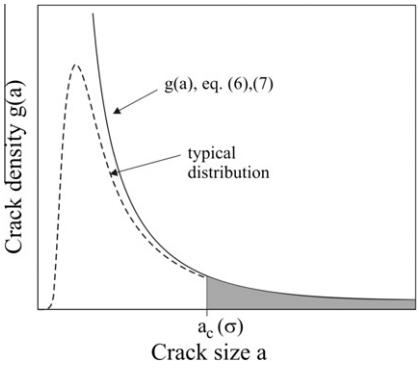

Fig. 2. Probability density of crack sizes a. The function $g(a)$ adopted by Danzer et al. [27] shows the distribution necessary for a Weibull distribution. For increasing stress σ the critical size of destructive flaws $a_c(\sigma)$ decreases, and the density of destructive flaws, indicated with the shaded area, will increase.

3. Lattice model

Over the years we have attempted to derive a better understanding of fracture in concrete and other brittle disordered materials by means of experiments and simple lattice-type model simulations of fracture derived from methods used in statistical physics ([13,14,28–30]). These network models were used several decades earlier to solve problems in elasticity [31], but the statistical physicists showed that crack patterns could very well be simulated with a simple model where fracture was mimicked by removing elements from the original lattice after certain strength or deformation criterion was met. We made the model fit to include the concrete material structure at the meso-level. Here there was a strong advantage compared to models based on FEM adopting solid elements, namely, the particle structure overlay of the material was achieved directly without using elements with complicated shapes as, for example in [32]. This advantage, together with the possibility to use a simple 1-dimensional fracture law for the beam elements made the lattice to an excellent tool for simulating, and in some cases even predicting [33,34], crack patterns in concrete specimens subjected to all-kinds of loading histories.

At the meso-scale the particle structure of concrete is recognized. The typical size-scale is (mm). Descending the dimensional scales, the micro-level is considered the next important size-scale for cement and concrete. At this scale the fine detail in the cement structure is considered at (μm)-size-scale. The dimensional size-scale could be reduced further to the (nm)-level, where the structure of hydrated cement paste comes into play. In this paper, however, we limit the analyses to the (mm)-scale, or the meso-level, and only the geometry of the aggregates in the concrete are included in the analyses. All detail at lower scales is simply ignored, and cement, aggregate, and the interfacial transition zone between aggregate and concrete, which are the three material phases generally considered in meso-level analyses, are simply represented as a continuum. This is a common assumption in almost any (multi-scale) model: at the lowest observational scale continuum assumptions must be made. Generally this is no problem when the material at that scale can be considered elastic (or plastic). The three phases are assumed to break in a brittle manner, meaning that at the meso-scale the three material phases have an elastic-purely brittle behaviour and no softening is considered. One may of course debate whether this assumption is correct, see for example [24], but it fulfils the requirement of simplicity, and as will be shown, can be quite helpful in elucidating the fracture process in different types of concrete, or rather 'numerical' concretes. Instead of using a statistical distribution of local properties (E, σ_c, or other), a particle overlay representing the real material works quite well and appears to lead to more realistic crack patterns [35]. In part this is so because geometric clustering of lattice elements with the same properties occurs by bringing in the material structure geometry. It is hard to determine what statistical distribution would resemble the disorder of a certain concrete, and already incorporating those elements that are known is quite helpful and further ads to the simplicity of the model. Energetically the match with fracture experiments is less good and many reasons can be put forward for the observed discrepancies. In the approach followed in this paper, this is, however, no real objection, since we are focusing on revealing the fracture mechanism when concrete, with varying composition, breaks in tension/flexure.

Numerous other models have been developed in recent years, either lattices, e.g. [20,36,37], employing brittle, softening [19,38] or classical fracture mechanics criteria (e.g. [39] for crack propagation, or particle-type model in the spirit of the Cundall and Strack model [40–42]. In the LEFM-based model of Wang and Huet [39] it

is essential to include pre-existing microcracks in the meso-structure. It was assumed that tiny cracks were present in the interfacial transition zone between cement matrix and aggregate particles. Most of these models are 2-dimensional. In recent years the lattice model has been developed in a completely 3-dimensional tool [43,44]. In its original form, computer-generated particle structures were used. The particles, usually circles (in 2D) or spheres (in 3D), followed a pre-defined size distribution. Most common has been to use a Fuller distribution, which gives the densest packing of particles with varying diameter. Particles were placed in a plane or in space using a random placement method; when a new particle would overlap with an already placed particle a new position was tried. The placement procedure is rather time consuming and it is good practice to omit all particles below a certain minimum size. It is assumed that these particles form an integral part of the matrix, which is assumed to behave like an elastic continuum. A minimum distance between particles was defined to allow for including an interfacial transition zone (ITZ, see below). In [33,43] details of the followed procedure can be found. A more general survey of existing models for including particle structures can be found in [45].

Recently it also has become possible to incorporate realistic particle structures using data from high resolution CT-scans of concrete prisms, which was one of the main parts of the doctoral thesis of the first author [44]. So the original size effect studies with the lattice model [46], which were carried out in 2D adopting a computer-generated particle structure of circular aggregates as described above, can now be done in full 3D and with a realistic particle structure of concrete, identical to that in practical concretes. For the sake of completeness we believe it is helpful to briefly summarize the particle overlay method and to say a few words on the used fracture law.

3.1. Particle overlay

A simple random or regular triangular lattice is projected on top of a previously composed material structure as mentioned above, or, as in this paper, on top of an experimentally determined particle structure. In this paper the lattice is always a so-called 'hcp-lattice', which is based on hexagonal close packing (hcp) of equal sized spheres. The hcp-lattice is shown in Fig. 3, and is always a regular triangular lattice. Obviously one may choose whatever is considered best. The element length used throughout the computations in this paper is 0.25 mm. Again one could comment that mesh sensitivity may appear in the matrix (see for example [47,48]). Since we are interested in comparing results of beams of different sizes, containing different shaped aggregates, as well as different volume fractions of aggregates, the lattice should be as simple as possible, and most importantly the same in all analyses. With that said, we accept that cracks follow a rather straight path in the matrix, knowing that this can easily be resolved by using a lattice with random beam length, or by using a statistical distribution of local matrix properties, where it should be mentioned that it is not so easy to determine which statistical distributions should be used. Again, we let simplicity prevail.

The scanning procedure is relatively simple. Computed tomography registers density differences, so the optimum way is to ensure large contrast between matrix and aggregates, for example to strive at a high density for the aggregate phase combined with a low density for the matrix phase (or vice versa). Useful aggregate material would be marble (ρ = 2700 kg/m^3) or basalt (3000 kg/m^3). Two different concretes were used in our study: one containing crushed basalt, the other oval-shaped basalt particles. The particle sizes ranged between 8 and 15 mm [44]. For the cement matrix CEM I 42.5 was used with a w/c-ratio of 0.3, leading to a matrix with density ρ = 2200 kg/m^3, i.e. significantly lower than that of the basalt. The aggregate content was varied, and was 20%, 30% or 40% for crushed aggregates and 40% and 48% for oval-shaped aggregates. The concrete was made more workable by adding a super-plasticizer (Glenium Stream, BASF). An example of a cross-section of a concrete prism scanned at the University hospital in Zurich (CT scanner: Siemens SOMATOM Definition) is shown in Fig. 4. The high-density aggregates appear white in the low-density matrix, which is grey. The pores, as well as the empty space surrounding the prism appear as black. The result from a complete scan is a stack of 2D images that can be reconstructed to the full 3D particle structure in Fig. 5 using open-source software developed by Rosset et al. [49]. The overlay of the scanned microstructure on the lattice is now quite straightforward. First the original image is transformed in a binary one. The three-dimensional nodal structure of the lattice in Fig. 3 is considered arranged in a stack of planes in the 3rd dimension. Each sub-sequent image of the scan corresponds with a plane in the 3D nodal stack of the lattice. Fig. 6 shows the principle. The procedure for assigning material properties to the various lattice elements is then as before.

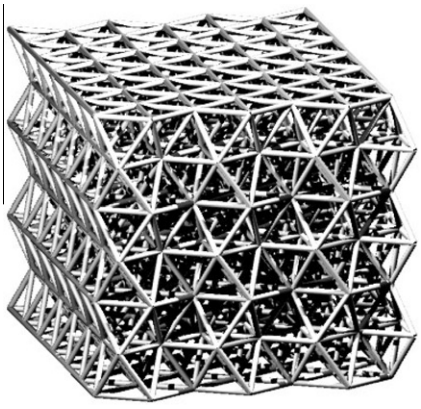

Fig. 3. Regular triangular lattice based on hexagonal close packing of equal-sized spheres.

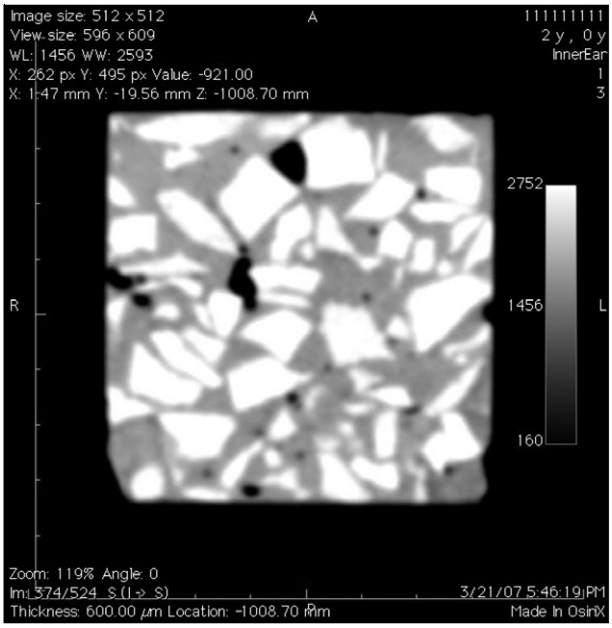

Fig. 4. CT-scan of a concrete prism containing crushed aggregates. In the cross-section shown, the lighter the grey, the denser the material. Dense basalt aggregates are visible as almost white, cement–matrix appears as grey and porosity is black.

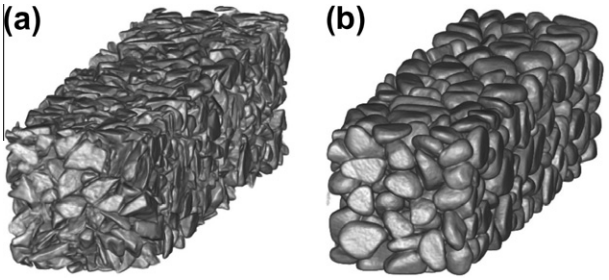

Fig. 5. Reconstructed particle structures for two concrete prisms: (a) crushed aggregates and (b) oval-shaped aggregates. The particle density is 45%.

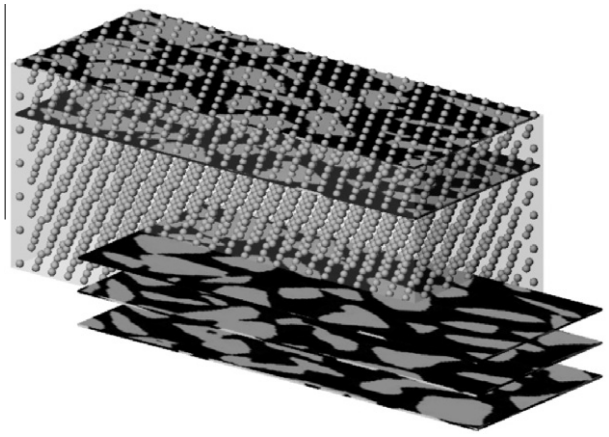

Fig. 6. 3D scheme showing the overlay of the lattice with the sub-sequent images from the CT-scan.

Elements with two nodes in the matrix will get matrix properties, elements with both nodes in the aggregate phase are assigned aggregate properties, and elements with one node in the matrix and the other in the aggregate phase are given properties corresponding to the interfacial transition zone or ITZ. An example of a scanned prism transformed in a lattice is shown in Fig. 7. The original particle structure is shown in Fig. 7a, the resulting lattice in Fig. 7b. These images reveal immediately one of the problems encountered, which is directly related to the resolution defined by the length of the lattice beam elements. In the present analyses this length was set to 0.25 mm. Consequently, when two aggregate particles are closer together than the lattice beam length, the ITZ that should be in between is lost, and the two aggregates 'melt' together. To some extent this can be avoided by choosing a shorter lattice beam length, but likely a better solution would be where individual aggregate particles are identified as such and to adjust the lattice accordingly. Obviously this adds further complications and the original elegance is lost. Therefore we simply allow the contact between aggregate particles to occur and consequently there is a loss of ITZ-phase in the concrete structure. Since porosity, at least the larger air voids, show up in the CT-scan, the porosity could also be included in the lattice by simply removing those lattice elements falling in the black pores. Since we will not include porosity in the present analyses, the interested reader is referred to [44] for more detail pertaining to the inclusion of porosity in the lattice. The same method can be used for modelling foamed cement, where no aggregates are included but only large pores, [50].

Due to the constant lattice beam length of 0.25 mm, the size of the ITZ corresponds to that. This is larger than what the actual size of the ITZ is generally assumed to be, viz. 30–40 μm. The positioning of the ITZ beams between the aggregate and matrix leads to a decrease of both the aggregate and matrix phase in the whole specimen, as indicated in Table 1 for the material compositions analyzed in this paper. The shorter the lattice beam length, the smaller the actual loss. Yet, decreasing the beam length leads generally to a large increase in number of elements, and with that to a large increase in computational effort, see [50–52].

3.2. Fracture law

The fracture law is very important. It decides when lattice beams are removed. Removing the lattice beams is done sequentially (event-by-event method) upon reaching a certain criterion. In the past, in 2D analyses we have used a fracture law based on bending moment and normal force in a lattice beam. When the maximum tensile stress due to normal force and bending exceeded the threshold stress, set for each of the three material phases, the

Table 1
Particle content from scanned specimens ($P_{k,sample}$), and after lattice overlay ($P_{k,lattice}$). The last column shows the amount of interfacial transition zone (ITZ).

Aggregate shape	P_k (%)	$P_{k,sample}$ (%)	$P_{k,lattice}$ (%)	ITZ (%)
Crushed	20	28.41	20.98	11.99
	30	37.93	29.17	16.26
	40	49.32	39.51	19.45
Oval	40	45.54	41.46	13.37
	48	53.43	47.81	15.12

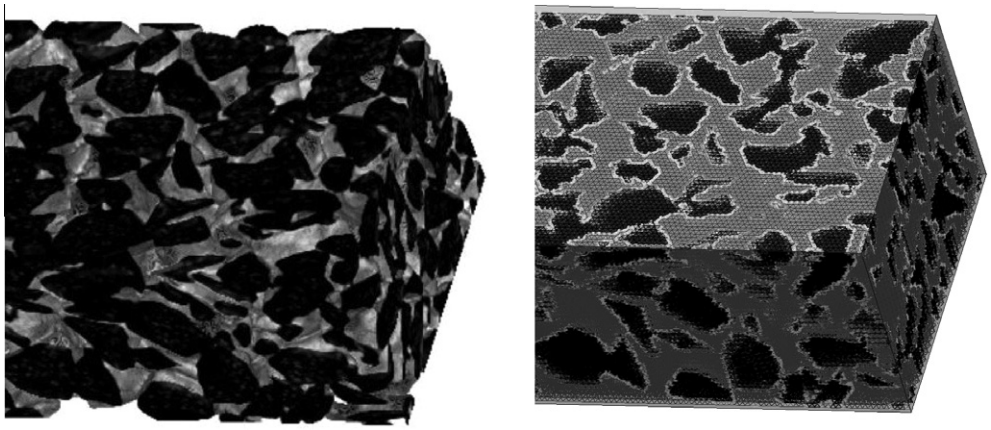

Fig. 7. Right part of scanned concrete specimen containing 40% crushed aggregate particles (a) and resulting lattice model (b).

element would simply be removed from the lattice and a new test-load would be applied. This implies that not, as is common in non-linear finite element analyses, the mesh is relaxed and the load that was originally in the removed beam would be re-distributed over the neighbouring elements. It has been argued, [53], that for non-proportional loading paths a more advanced redistribution is essential. For proportional loading, though, the event-by-event method would give correct results.

In 3D lattice it becomes more tedious to take into account the bending effect. Not only are there two bending moments (M_x and M_y if the z-axis is oriented in the direction of the beam axis); one should also decide what to do with torsion. We therefore returned to a criterion based on normal load only; any rotation due to bending or torsion is ignored. The removal criterion thus becomes very simple indeed:

$$\sigma = \frac{N}{A} \leqslant f_t. \tag{8}$$

The required input parameters for the lattice analysis are then limited to six parameters, E_i and $f_{t,i}$ (where i stands for the aggregate (a), matrix (m) or ITZ phase), which reduces to 5 when the Young's modulus for the ITZ and the matrix are assumed to be equal. In the present analyses $E_a = 70$ GPa, $E_m = E_{ITZ} = 25$ GPa and the strength thresholds: for aggregate, matrix and ITZ $f_{t,a} = 10$ MPa, $f_{t,m} = 5$ MPa and $f_{t,ITZ} = 1.25$ MPa, respectively. These values all correspond to what was used before, [33,34]. Note that the ratio of strength and stiffness matters, not so much their absolute values.

Table 2
Geometries of the prisms and number of lattice elements for each size.

Prism	Size (mm^3)	# Elements
'A'	$6.25 \times 2.38 \times 2.6$	21,107
'B'	$12.5 \times 4.6 \times 4.8$	143,627
'C'	$25 \times 9.31 \times 9.53$	1155,549
'CD'	$37.5 \times 14.32 \times 14.5$	3906,967
'D'	$50 \times 18.84 \times 19.04$	9269,081

Table 3
Number of simulations carried out for prisms 'A' through 'D'. Size 'CD' is an intermediate size between 'C' and 'D' (see text).

P_k (%)	Aggregate shape	'A'	'B'	'C'	'CD'	'D'
20	Crushed	10	10	6	–	1
30		12	8	8	1	1
40		12	8	6	1	1
40	Oval	12	8	5	1	1
48		12	8	5	1	–

3.3. Overview of analyses performed

In the analyses a parallel version of the lattice model was used; the parallel solver was developed by Lingen [54]. As mentioned fracture in prisms loaded in three-point bending was simulated. The size of the prisms was dictated by the available computing infrastructure: SGI Altix 350 (16 single core Intel Itanium 2 processors), which we had available in our Institute, the HP Superdome of ETH Zurich (96 dual-core Intel Itanium 2 processors) and the CRAY XT3 at the CSCS in Manno, Switzerland (with up to 1656 dual-core AMD Opteron processors). The last two facilities were used for the largest, multi-million element analyses, the local workstation was used for the smaller problems. A test problem run on CRAY showed that the parallel solver could be used well when between 128 and 256 processors were used. The efficiency decreased with further increasing number of processors, see [44].

The concrete prisms, which were subjected to three-point bending, have dimensional ratio's $l \times b \times h \approx 2.6 \times 1 \times 1$. The absolute sizes for prisms 'A' through 'D' are given in Table 2. Note that one additional size 'CD' is included. Instead of doubling the size from 'C' to 'D' by a factor 2, only an increase by a factor 1.5 was made. The reason is simple: the necessary computer infrastructure was not available at the time that the BSc-thesis [51] was completed. The prisms are rather stubby, which again was caused by the desire to reduce the number of elements in the computations. Also for computational reasons, a larger number of smaller specimens were analysed, compared to only one for the 'CD' and 'D' specimens (see Table 3).

Going from size 'A' to 'D' the up-scaling factor is 8. Note that the smallest specimens are indeed small compared to the maximum aggregate size (15 mm) in the concrete. The smallest prisms 'A', but also the next smallest prisms 'B', are not representative volumes in the spirit of continuum theory. In meso-scopic analyses, where the complete meso-structure is included, this is, however, no problem. The consequence is that in these meso-scopic analyses scatter will be larger for the smaller prisms, which is an argument to have a larger number of repetitions for the smaller sizes than for the larger ones. The specimens were cut from the larger scanned concrete prisms. Fig. 8a shows how three prisms of size 'D' can be cut-out. The smaller sizes 'A' through 'C' were cut-out from the 'D' prisms, keeping one reference point at the lower edge of the front face (see Fig. 8b). Thus, the concrete meso-structure is the same along (part of) the front lower edge of the specimens. The material structure is different everywhere else, which is caused by the three-dimensional scaling. Therefore, crack initiation in beams of different sizes can be compared along part of the lower front edge only. In physical experiments even this would be impossible since the grain structure cannot be easily controlled. This is another advantage of the simulations, even though they are no more than an approximation of reality. In all crack maps shown

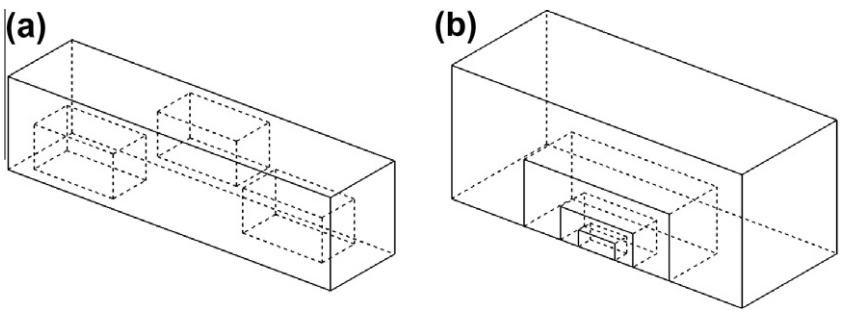

Fig. 8. Cutting prisms of size 'D' from scanned concrete samples (a), and cutting the smaller prisms 'A', 'B' and 'C' from the largest prism 'D' while keeping the centre point on the lower front edge as constant reference (b).

in this paper the prisms are oriented to show the lower front edge most clearly.

4. Size effect and damage distribution from lattice analyses

4.1. Size effect on strength

As mentioned in the introduction size effect on structural strength is still open to debate. Here we would like to relate the observed strength decrease with the fracture process observed in specimens of different size. These results are still rather preliminary: we show some observations, and sketch a possible strategy to return to a simplified macroscopic engineering model. Up till now we have studied the crack development in the analyses mentioned in Table 3. Two examples of load–displacement diagrams are shown in Fig. 9, one for oval-shaped aggregates (Fig. 9a), and one for crushed aggregates (Fig. 9b). The displacement is the mid-displacement directly under the load-point. The two examples relate to an aggregate content P_k = 40%, for size 'C', the next largest size. Three stages of cracking (a–c), are identified along the load–displacement curves. These stages relate to the crack patterns shown in Fig. 10. Fig. 10a–c shows the cracking on a plane well inside the prism for oval-shaped aggregates, whereas Fig. 10d–f show cracking for crushed aggregates. The dashed lines show the size of the

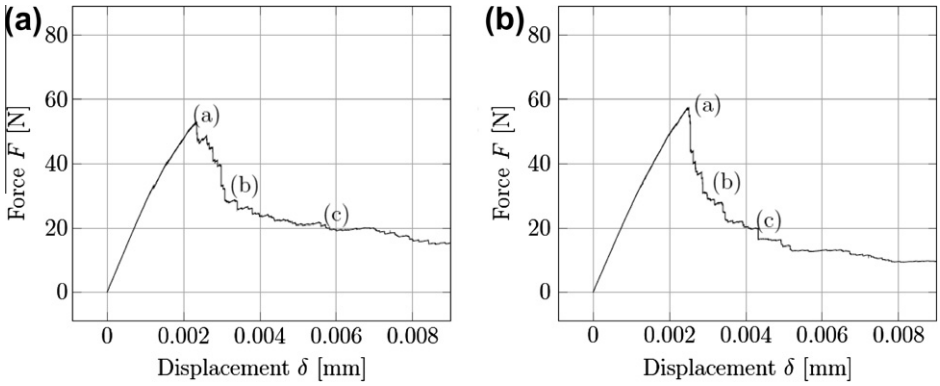

Fig. 9. Calculated load–displacement diagrams for prisms of size 'C' with an aggregate density P_k = 40%. Figure (a): oval-shaped aggregates; figure (b): crushed aggregates. The stages (a) through (c) along the curves show the positions of the crack patterns shown in Fig. 10.

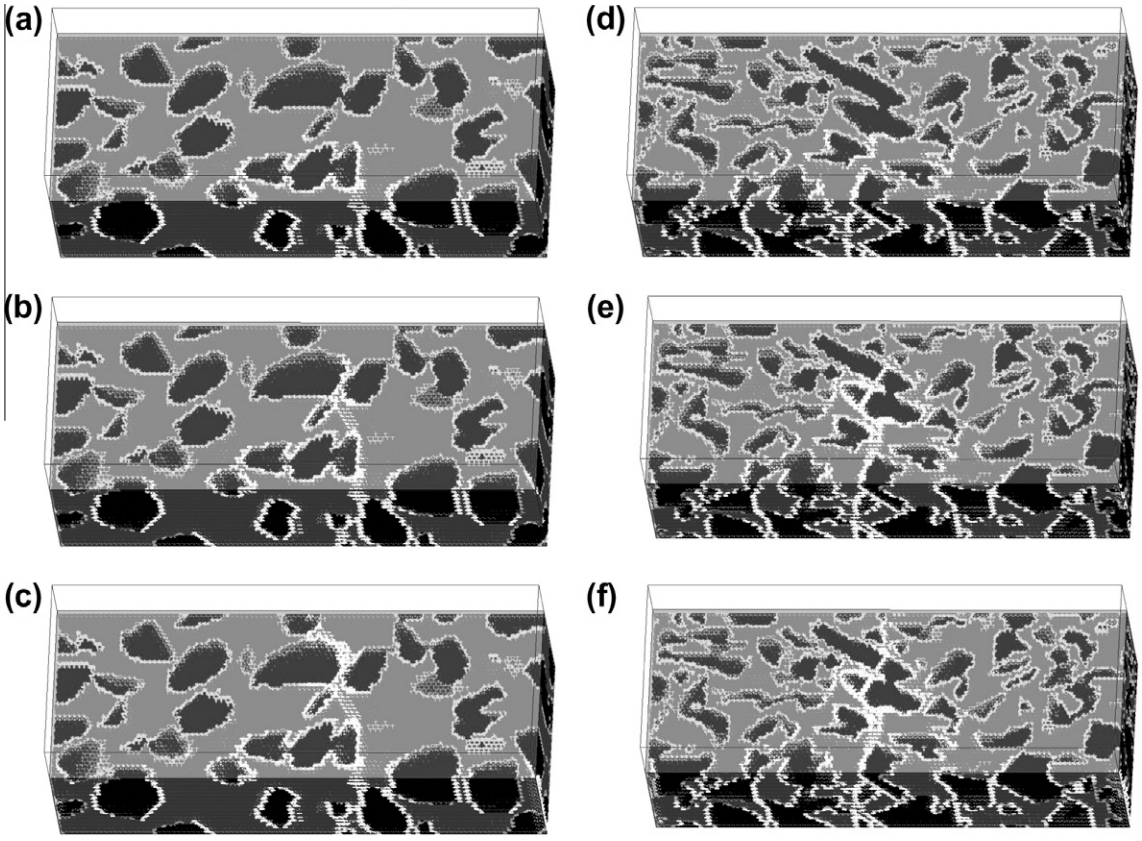

Fig. 10. Crack history for the two simulations on size 'C' prisms of Fig. 9. The crack patterns of the analysis with oval-shaped aggregates are shown in figures (a)–(c); for the analysis with crushed aggregates in figures (d)–(f). The three stages, from top to bottom are: peak–load F_{max} (stage (a) in Fig. 9), approximately $0.6F_{max}$ (post-peak) (stage (b) in Fig. 9), and approximately $0.4F_{max}$ (post-peak) (stage (c) in Fig. 9).

complete prism and helps to identify where the image are located. At peak-load, (Fig. 10a and d) we see that interfacial cracks have developed along the lower surface of the entire beam. At this stage, only very few matrix beams are cracked (see also the next section), and no aggregate beams at all. This is no surprise considering the ratio 10:5:1.25 for the aggregate to matrix to ITZ strength. At stage (b) we are well in the post-peak regime, and the ITZ cracks appear to join and form a localized macro-crack (Fig. 10b and e). The number of matrix cracks increases (see the next section), and now also some aggregates are broken. In the prism with crushed aggregates these particles are just below the load point (Fig. 10e). Obviously it is easier for the material to allow the main crack to cross the aggregates, rather than to grow around them. The stress-concentrations in the irregularly-shaped crushed aggregates allow for the aggregates to break, which does not appear, or to a lesser extent, when rounded or oval-shaped aggregates are modelled. Finally, in stage (c) we see that the main macro-crack has grown almost completely through the prism, up to the loading point (crack patterns: Fig. 10c and f). Surprisingly, as we will show quantitatively in the next section, the total number of cracks decreases when we load further in the softening regime, and it appears that no isolated cracks develop further outside the main crack. The decrease of the total number of cracks is then likely caused by 'eating-up' of smaller cracks in the trajectory of the main macroscopic crack, and or joining of individual ITZ cracks through the growth of matrix cracks in between to one larger crack. So, at this stage a preliminary conclusion can be drawn: no 'microcrack' cloud appears to precede the growth of the macro-crack, as is assumed in some of the cohesive crack models as a plausible explanation for softening, e.g. [55]. Instead, the severe micro-cracking seems to be limited to the pre-peak regime; at peak load the microcrack pattern is more-or-less fully developed, and beyond peak, in the softening regime, we only see the growth of a single macro-crack, with perhaps some crack-joining events leading to the observed decrease of total number of cracks. This implies that the load-peak can be interpreted as marking a 'phase'-shift: from a material containing distributed microcracks displaying 'continuum-like' behaviour to a material with one single dominant macro-crack in the spirit of classical fracture mechanics, which should be enhanced to incorporate crack-face bridging, however. We will return to these matters in Section 4.2 and in the discussion in Section 5 thereafter.

The results shown up till now all relate to prism size 'C'. It is interesting to look to differences between prisms of different size. In Fig. 11 we show the crack patterns for P_k = 20%, crushed aggregates, in sizes 'A' through 'D'. The crack patterns are shown at F_{max} (peak) and post-peak at approximately $0.40F_{max}$. The same crack process as sketched above can be recognised in most sizes, except perhaps for the smallest size 'A'. Here we see that a few large aggregates make up most of the specimens, and thus, the fracture behaviour is very dependent on the accidental location of the weak interface elements. When looking to the largest size 'D' it is quite clear that at peak mostly ITZ cracks have developed along the lower part of the prism, with perhaps a few matrix cracks. Subsequently, at $0.4F_{max}$ in the softening regime, we see the development of a few major cracks, and only limited development of further ITZ cracking (some appear at the right side of the main cracks, at about half height of the prism). We will return to the discussion of the fracture process in Section 4.2 where the crack statistics will be summarized.

Size effect on nominal strength is usually shown in bi-logarithmic log σ_N–log D plots. In Fig. 12 the results are shown for P_k = 40%, for oval-shaped particles (Fig. 12a) and for crushed aggregates (Fig. 12b). Instead of showing the prism height along the x-axis we show the prism volume V, which relates better to Eq. (2). Although scatter is large in the smallest size specimens, caused by the extreme ratio of aggregate size and prism height, we still include the results in the analysis. It is possible to calculate the negative slope of the best-fit straight line through the data points, following,

$$\ln \sigma_N = a + b \ln V, \tag{9}$$

with a and b the intersection point with the σ-axis and the (negative) slope of the regression line, respectively. In Table 4 and in Fig. 13 the results are summarized for the different particle densities and the two different aggregate shapes. For crushed aggregates, the slope of the regression lines vary between −0.15 and −0.18. Using in Eq. (1) a Weibull modulus m = 12 from Ref. [56], which fits well for the size-effect experiments summarized in [57] in a range of 1:32, for 3D-scaling the slope would be $m = -3/12 = -0.25$. A Weibull modulus of 6,7 would be in agreement with the data of Table 4. It is quite obvious that one of the parameters deciding the value of m is the particle density, the second factor being the type of aggregate (crushed, oval-shaped, etc.). It has to be mentioned that the size-range studied

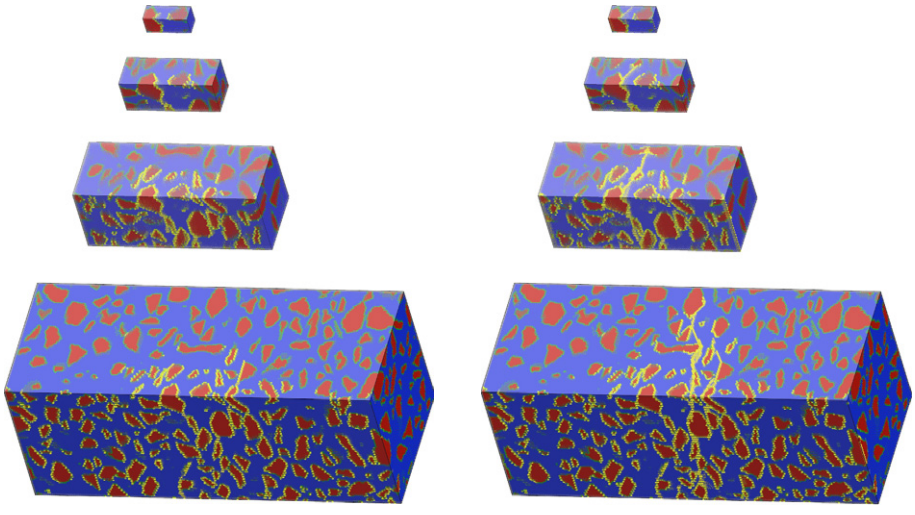

F_{max} $0.4F_{max}$ (post-peak)

Fig. 11. Crack growth in prisms, sizes 'A' through 'D' (top to bottom; scaling 1:8), with P_k = 20% oval-shaped aggregates. In the left column the crack population at peak–load F_{max} is shown, in the right column at $0.4F_{max}$ (post-peak).

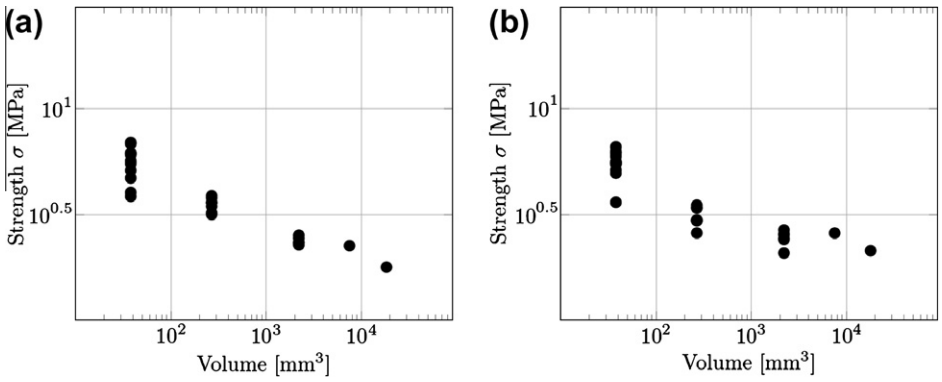

Fig. 12. Bi-logarithmic plots of nominal strength σ_N vs prism volume V for: (a) oval-shaped and (b) crushed aggregates. The particle volume is $P_k = 40\%$.

Table 4
Regression coefficients, confidence intervals (*CI*) and correlation factors *R* of size effect analysis according to Eq. (9). The slope *b* is shown graphically in Fig. 13.

Aggregate shape	P_k (%)	a	$CI(a)$	b	$CI(b)$	R
Crushed	20	2.16	0.152	−0.17	0.026	−0.90
	30	2.09	0.186	−0.15	0.033	−0.85
	40	2.27	0.166	−0.18	0.02	−0.90
Oval	40	2.36	0.148	−0.19	0.026	−0.94
	48	2.66	0.229	−0.24	0.04	−0.91

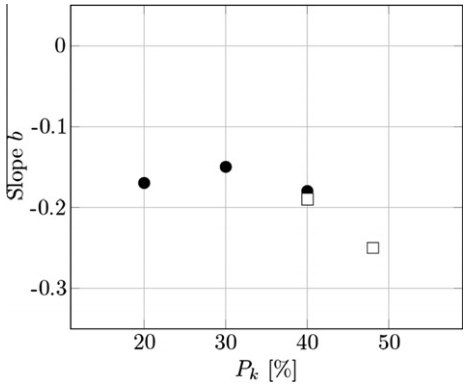

Fig. 13. Effect of the aggregate density P_k on the slope b of Eq. (9); data are shown in Table 4. The closed circles are the crushed aggregate mixtures, the open squares the mixtures with oval-shaped aggregates.

here is just 1:8. This is, without doubt, a narrow range (also considering that the smallest size is just about the same as the aggregate size). Excluding the smallest prism from the analysis leads to different values of the coefficient b, which then ranges between −0.07 and −0.12, and thus the values of the Weibull modulus m between 8 and 14. The graphical form does not change much from Fig. 13, just a shift in vertical direction of the entire graph, see [44]. The regression coefficients are around 0.90, which justifies the approximate analysis we carried out. More analyses would be needed to further secure these results, but the computational effort would be demanding, not so much the higher number of repetitions of the smallest prisms (although likely a few hundred realisations would be needed considering the large variations in material structure), rather the analysis and the necessary repetitions of prisms a factor 4–8 larger than the current 1:8 range.

4.2. Crack statistics

From the analyses all details regarding the state of cracking at all loading stages from the beginning to full rupture are known. It is thus possible to analyse the data in the spirit of the work by Danzer et al. [27], which was shown in Fig. 2. Quite some work is needed, however, to extract cracks sizes, where one should remember that the cracks are curved surfaces. In an earlier paper we looked to crack densities in 2D: crack lengths were simply determined as the length of a line connecting two crack tips [17]. Here a different procedure is followed, where the tortuosity of the crack surfaces is preserved. In Fig. 14a and b the crack pattern is shown in two different manners. The extracted pattern of Fig. 14b forms the basis of the analysis. A 3D cubic grid is superimposed on the crack pattern (Fig. 14c); the smallest size of a grid element is one lattice beam length, the largest size equals the smallest dimension of the calculated prism. Next, those cubes containing a crack are separated from those without cracks (Fig. 14d). Following this extraction, it is checked which cubes have neighbours, and thus are part of a larger crack plane. In 3D each grid cube has 26 neighbouring elements, which reduces to 8 when all diagonal connections are neglected. Clusters of cubes thus form a single continuous crack, which can be coded with a unique colour[1] or grey-tones (Fig. 14e). Finally, the largest crack can be extracted (Fig. 14f), and also the crack size distribution can be plotted, this all at various stages of the loading history.

Here we show the results for the specimens with crushed aggregates, $P_k = 40\%$, only: once for each prism size ('A' through 'D'). In Fig. 15 all resulting crack size distributions are summarized. In all but the smallest size 'A' the tail region of the distribution is shown in a separate box, which helps to identify the largest crack surface. The crack sizes as a ratio of the total cross-sectional area of a certain prism are gathered in Table 5. Qualitatively the distribution resembles the one hypothesized in Fig. 2. There are many small cracks, and only a few long cracks. The largest crack keeps growing in the post-peak regime (compare the peak and post-peak stages for all sizes); the total number of cracks gradually decreases, which is due to the fact that several smaller cracks may join to form a large crack. It also indicates that not very many new smaller cracks will nucleate in the softening regime, as also shown in Table 6, which shows the number of cracks counted at F_{max} and at $0.4F_{max}$ in the softening regime. This is in contradiction to assumptions made in cohesive crack models, e.g. [55]. In such models it is normally *assumed* that 'a cloud of microcracks' progresses ahead of a growing macro-crack. Here the emerging picture is different: the prisms are first 'weakened' by the growth of many distributed microcracks, which occurs till peak load is reached. Subsequently one of the largest microcracks will become critical, starts to grow and may likely join with other smaller cracks to form the final macro-crack. This is not necessarily limited to one large crack

[1] For interpretation of colour in Figs. 1, 11, 17, the reader is referred to the web version of this article.

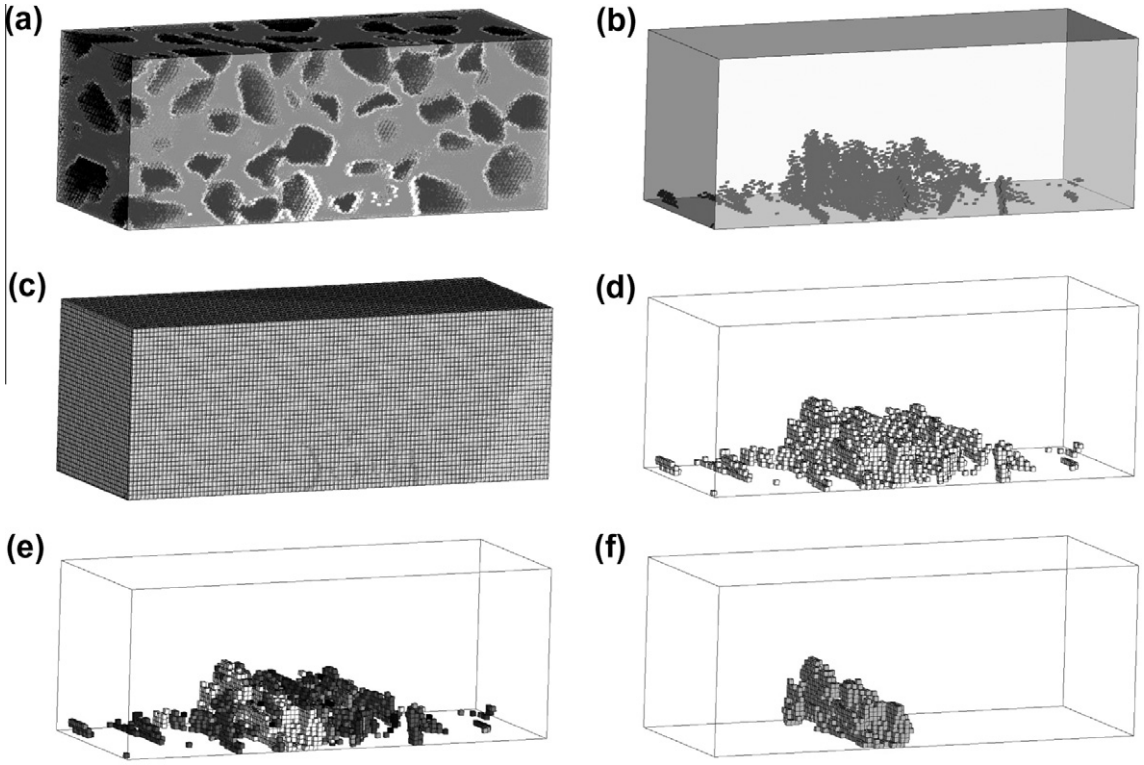

Fig. 14. Procedure developed for calculating the crack size distribution from three-dimensional lattice analysis. Figure (a) and (b) show the cracked prism. In figure (b) only the removed elements are shown. A three-dimensional grid is superimposed on the prism, and boxes containing a crack are labelled, see figure (d). Continuous cracks are defined when neighbouring boxes are also filled (see main text), and clusters of removed elements thus form continuous crack planes (e). The largest crack can be easily found, and is shown in figure (f).

during the crack growth phase, but several larger cracks may grow simultaneously, as can for example be seen in prism 'D' in Fig. 11b. It must be emphasized again that the number of results is too small to arrive at final conclusions, but the fracture process is much in line with earlier studies focussing on cracking in tensile experiments, see for instance [17,33,43,46]. The fracture process described here forms the basis for the so-called 4-stage fracture model [58,59].

The above crack size distributions do not say anything about the location where a crack is situated, i.e. in the matrix, aggregate or ITZ. This information can also be extracted from the analyses, and helps to characterize the fracture process as well. In Fig. 16 we show the crack ratio's in the analyses with 40% crushed and oval-shaped aggregates. The crack ratio's show the distribution of cracking in the ITZ (middle grey), matrix (light grey) and aggregate (dark grey) phase of the concrete at 4000-loading-step-intervals. Along the uppe edge of the diagrams the stages (a–c) are identified, which correspond to the marked stages in Fig. 9. In both cases, viz. crushed and oval-shaped aggregates, the fracture process starts with the nucleation and growth of ITZ cracks. Just before stage (a) is reached (the peak load), also matrix cracks start to develop. Aggregate cracks are relatively more abundant in the material with crushed aggregates, and appear just a bit earlier, i.e. already at peak load. The observations are in agreement with those in [43] for uniaxial tension.

5. Discussion

The results presented in this paper clearly show that the fracture process in (numerical) concrete is different from the normal assumptions made in cohesive crack models, for example [55]. Often in phenomenological models *assumptions* are made about crack mechanisms that are in no way supported by the analyses made. In cohesive crack models all is based on energetic analysis of the fracturing of structures, without giving much attention to the real fracture process. This is no surprise since the details of the material structure are not considered in such models: the material is handled as an isotropic continuum. For materials like concrete, with a highly heterogeneous material structure, a continuum approach is highly debatable, especially when specimens are so small they cannot be considered as representative volume elements. In [18] we list a number of cases where the ratio between smallest structure size and maximum aggregate size is barely larger than one, i.e. similar to prisms of size 'A' in this paper. The difference in approach is that here we include all detail of the material structure, whereas in the continuum-based size effect laws nobody seems to worry whether the structures are larger than, say, a factor 8–10 as the RVE. Neither is it common to use a statistical distribution of continuum properties. Of course for a material like concrete, with its rough aggregate structure, it is difficult to comply with this demand, especially when physical experiments are carried out in the lab.

In the analyses presented in this paper we had to limit the structural size range to 1:8 because of computational reasons. Computer infrastructure development in the last few decades has certainly been startling, and compared to the 2D-lattices of 3000 elements that we studied in the early 1990s [15], we can now perform multi-million element analysis of fully 3D-problems with incredible detail in the material's meso-structure (the increase corresponds more-or-less to what should have been expected based on Moore's law). In spite of this progress, it is still not enough. The largest 'D' sizes could only be analyzed once on the largest computer available to us. We would be interested to increase

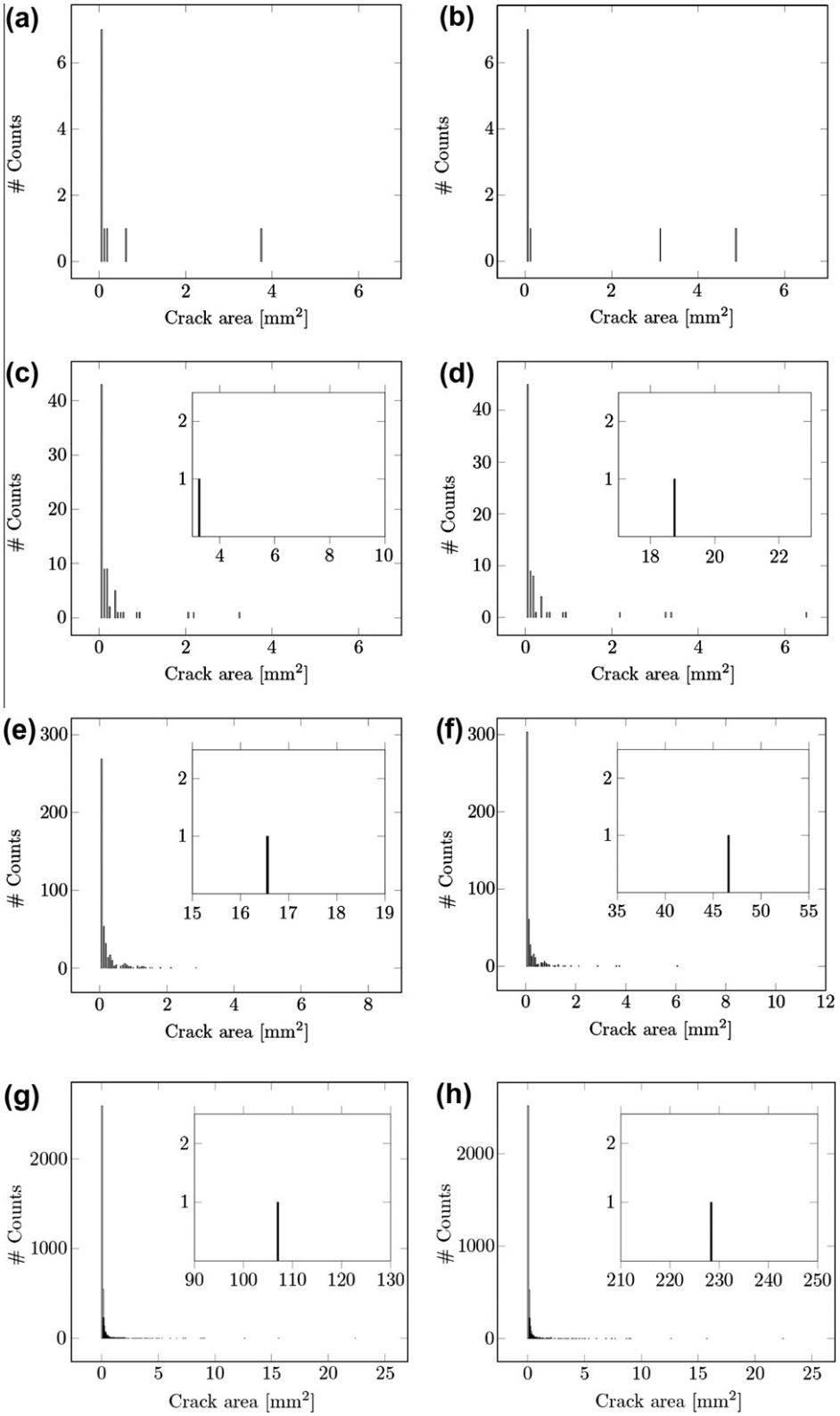

Fig. 15. Crack size distributions in prisms of four different sizes ('A' in figures (a) and (b), 'B' in (c) and (d), 'C' in (e) and (f) and 'D' in (g) and (h)), for 40% crushed aggregates. The crack densities are shown at two loading stages: F_{max} (figures (a), (c), (e) and (g)), and at $0.40F_{max}$ in the post-peak regime (figures (b), (d), (f) and (h)). Note that the *x*- and *y*-scales are different for each prism size. For each size the diagrams have the same scale for the peak and post-peak distributions.

scaling at least to 1:64, preferably even larger, with multiple repetitions for each size. Another wish would be to include more realistic ITZ thickness, which would increase the amount of material structure detail, but which is impossible using today's computing infrastructure, unless very small specimens are considered.

So, what have we learned in the past two decades? The size of the problems has increased by a factor 1000; the model is fully 3D and realistic aggregate structures have been included. The progress has been in the understanding of the fracture process. In the beginning it has become clear, almost immediately, that

Table 5
Largest crack size a_{max} relative to the cross-sectional area A of a prism ('A' through 'D') at peak load and in the softening regime at 40% of peak load. The aggregate density P_k = 40%, crushed aggregates.

Prism size	a_{max}/A at F_{max}	a_{max}/A at $0.4F_{max}$ (post-peak)
A	0.61	0.79
B	0.43	0.75
C	0.19	0.48
D	0.25	0.55

Table 6
Number of cracks at F_{max} and $0.4F_{max}$ (post-peak), for two different crack densities; crushed aggregates.

P_k (%)	Prism size	# Cracks at F_{max}	# Cracks at $0.4F_{max}$ (post-peak)
20	A	9	12
	B	73	66
	C	472	413
	D	4366	3621
40	A	11	10
	B	77	77
	C	509	475
	D	4308	3619

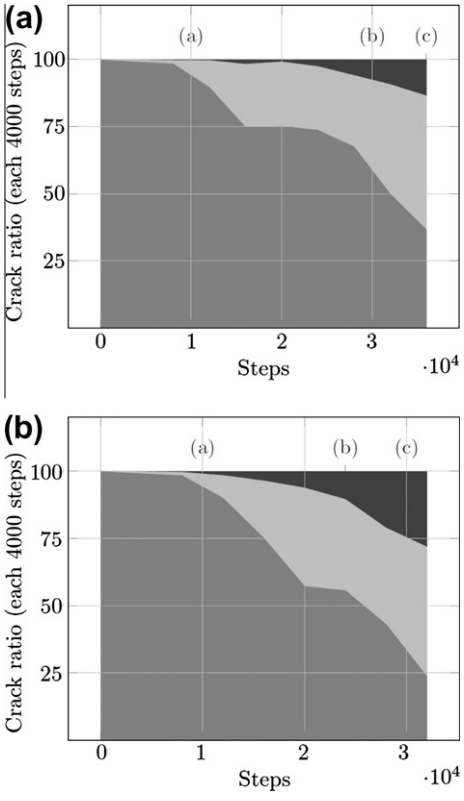

Fig. 16. Number of removed (failed) ITZ (middle grey), cement matrix (light grey) and aggregate (darkest grey) lattice beams, failing at various loading steps for oval-shaped (a) and crushed aggregates (b). The aggregate density P_k = 40%, the prisms size is 'C'. The stages (a), (b) and (c) indicated in the diagrams correspond to the loading stages identified in the load–displacement diagrams of Fig. 9.

crack-face-bridging is an important mechanism explaining the tail of the softening diagram, e.g. [15,60]. Next the idea that macro-crack growth dominates the steep part of the softening curve [60], and finally that micro-cracking precedes all this in the pre-peak regime, e.g. [17]. The material structure has a significant effect on how micro-cracking develops, has an effect on the peak strength, and does influence the size effect on strength, as has all been shown in previous papers and the present one. Getting the load–displacement diagrams quantitatively correct, and less brittle still remains an open issue. Including more detail in the material structure, and extending in the 3rd dimensions have brought some small changes, but not as much as we would have liked to see. Consequently, deeper reasons that would explain the brittleness in physical terms must be found elsewhere, and likely a shift in basic assumptions is necessary. One way out of the problem may be to have a closer look to material structure, its geometry, and geometrical changes therein when mechanical load is applied. Geometrical changes may be understood as cracks. Calculating crack size distributions – as in this paper – is one of the first steps; comparing the results to high quality experiments would be the first next step. High resolution CT-scans can be made nowadays, revealing the internal damage in specimens under load, e.g. [50,61,62]. Another way out has been discussed in [24], namely the introduction of softening potentials at the micro- and meso-level. Until now this step has not been made since the first idea was to see what softening actually means in terms of crack nucleation and growth. Much of the detail has been revealed, and now a failure criterion should be sought that would solve the brittleness problem without affecting the fracture mechanism from distributed micro-cracking, to localised macro-cracking and finally to crack-face bridging. In doing so it seems important to realize that softening is for the largest part a structural property. Models using softening as a material property can almost immediately be dismissed as useless, unless a robust procedure is included allowing to determine a sort of 'computational softening' diagram, for example from inverse analysis. It should be shown that such a diagram can be established in a unique manner (which is not really easy). We believe that over the past decades there has been too little effort to change the course of research, too many stick to the idea of softening being a material property, and it has been obvious that predicting mechanical behaviour has been very difficult if not impossible with such models. Post-dictions have been the trend, but this is no more than curve fitting.

We realize that the lattice model that we use is not mechanically perfect. Several improvements need to be made, and time has come to address these matters.

The crack density results can be used to feed the 4-stage fracture model [58,59]. In this model macro-crack growth during the steep part of the softening curve is handled using classical fracture mechanics theory. The clear advantage is that the structure geometry and boundary conditions (in the present paper a prism subjected to three-point bending, with freely rotating supports) are included in the formulation, and thus softening is really treated as a combined material and structural property. For size 'C' we have calculated an 'effective' crack length, starting at a pre-peak loading of $0.8F_{max}$. The 'effective' crack length was calculated by projecting the result of the crack size distribution (Fig. 14e) on the back surface of the specimen, and then connecting the tip of the largest cracks and the bottom of the prism, as shown in the inset of Fig. 17. The length of the 'effective' cracks develops as shown in Fig. 17, for different densities of crushed aggregates and for oval-shaped aggregates. Considering that the height of the prism is almost 10 mm (see Table 2), the crack ratio can be calculated by dividing the absolute values by a factor 10. As can be seen, the ratio ranges between 0.39 and 0.55 for all concretes, which is close to the initial notch depth a/H = 0.5 originally proposed for the model experiments to measure the fracture energy of concrete for the fictitious crack model [63]. At $0.4F_{max}$ in the softening branch, we see that the 'effective' crack length has increased to 8.05–8.8 mm depending on aggregate type and content, and thus almost the entire cross-section of the prism is cracked. Still we can carry 40% of the peak load, which cannot be explained from the carrying

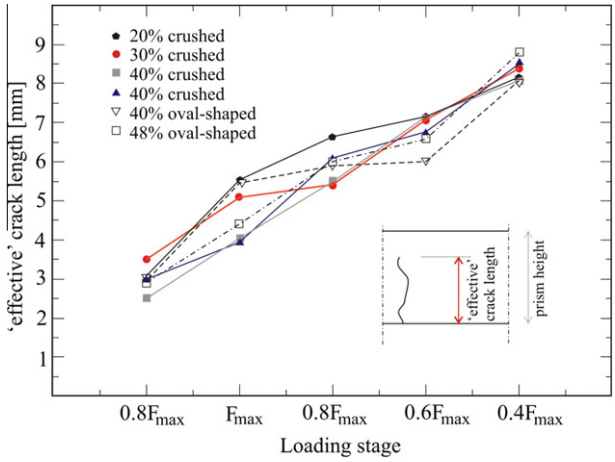

Fig. 17. 'Effective' crack lengths at various loading stages in size 'C' prisms. The 'effective' crack length has been derived from the crack density distribution at selected loading stages by simply connecting the tip as a projection on the back plane to the bottom of the prism as indicated in the inset.

capacity of the remaining ligament. This is exactly the bridging effect, which should be included in the 4-stage crack model as an internal pressure in the growing crack, however, not using shape of the entire softening diagram as closing pressure, but rather the tail of the softening diagram only [58]. To be debated is how the 'effective' crack length should be measured. The 3-dimensional crack front is not straight, and in an 'equivalent' 2D analysis we assume that the tip is straight in the 3rd dimension. In the end the micro-mechanics analysis is more precise, but an approximate macroscopic model in 2D would be useful under many circumstances. The 4-stage fracture model is based on true fracture mechanisms, and is to be preferred above many other models, including the still popular cohesive crack models.

6. Conclusions

In this paper results are presented from numerous 3D lattice simulations of fracture in prisms subjected to three-point bending. The originally proposed lattice model with a simplified normal stress criterion for fracture has been used. Realistic particle structures of concrete prisms have been obtained by making a CT-scan and projecting the obtained 3-dimensional image on an hcp-lattice. Different aggregate sizes have been studied, viz. oval-shaped and crushed aggregates, with varying densities in prisms of varying size (scale range 1:8). The results shed some light on the relation between crack size distribution and size effect on strength, be it that the size range is still too limited. Larger specimens, in full 3D could not be analysed due to computer infrastructure constraints. The following conclusions can be drawn.

(1) A size effect on structural strength was observed in all analyses, for all different concrete compositions.
(2) The size effect on structural strength can be approximated with a Weibull model; the Weibull modulus m depends on the type of aggregate and the aggregate density.
(3) The crack size distribution takes the same form as hypothesized by Danzer et al. [27]. At peak load always a large number of microcracks is found, and just a few larger cracks. The larger cracks are decisive for strength and softening behaviour. One of the larger cracks grows when loading is continued in the softening regime; no further microcracks seem to develop at that stage.
(4) The total number of cracks decreases in the softening diagram, which can be explained from crack-joining or from consumption of small cracks by the large macro-crack. The effect is larger for larger specimen sizes.
(5) The results from the meso-mechanical analysis with the lattice model can be used for feeding the 4-stage fracture model [58]. It is easy to demonstrate where bridging comes into play and from which point in the load-history macro-crack propagation is to be considered the main mechanism. The advantage of the 4-stage fracture model is that it incorporates both material and structural effects during softening.

Finally, further work is needed, and likely larger structures can be analyzed when a better computer infrastructure comes available. Extension to a size-scale of 1:64 is considered essential, perhaps even larger, with many repetitions per specimen size. The large brittleness of the lattice model needs now first more attention. Moreover there is a great need for high-quality tomography data of the fracture process in concrete, both in tension and compression, and for large specimens. Unfortunately the computed tomography technique is still best applicable for smaller specimens since otherwise the required resolution cannot be obtained. Also here technological improvement of the experimental tools is essential for progress in the field. As a matter of fact working on new experiments is considered far more important at the moment than developing 'new' models that lack a solid physical basis with a sole justification being to facilitate engineering analyses. Engineers would certainly benefit from physically-based models, which are critically lacking for concrete fracture.

Acknowledgement

The analyses at the Swiss National Supercomputing Centre (CSCS) in Manno were possible through a grant under project number ID s147. We acknowledge with gratitude this support. Moreover, we would like to thank Dr. Patrick Stähli for his excellent help in making the concrete specimens and his assistance with the CT scan. We are grateful to the staff of the University Hospital for their help, not in the last place for allowing us to have a concrete 'patient' in the CT-scanner.

References

[1] Walsh PF. Fracture of plain concrete. Indian Concr J 1972;46(11):469–70.
[2] Bažant ZP. Size effect in blunt fracture: concrete, rock, metal. J Eng Mech 1984;110:518–35.
[3] Carpinteri A, Chiaia B, Cornetti P. On the mechanics of quasi-brittle materials with a fractal microstructure. Eng Fract Mech 2003;70:2321–49.
[4] Burgoyne C, Scantlebury R. Why did Palau Bridge collapse? Struct Eng 2006;6:30–7.
[5] Bažant ZP, Yavari A. Is the cause of size effect on structural strength fractal or energetic statistical? Eng Fract Mech 2005;72:1–31.
[6] Shioya T, Iguro M, Nojiri Y, Akiyama H, Okada T. Shear strength of large reinforced concrete beams. ACI SP 1989;118:259–79.
[7] Dempsey JP, DeFranco SJ, Adamson RM, Mulmule SV. Scale effects on the in-situ tensile strength and fracture of ice. Part I large grained freshwater ice at Spray Lakes Reservoir, Alberta. Int J Fract 1999;95:325–45.
[8] Dempsey JP, Adamson RM, Mulmule SV. Scale effects on the in-situ tensile strength and fracture of ice. Part II first-year sea ice at Resolute N.W.T. Int J Fract 1999;95:346–78.
[9] Weibull W. A statistical theory of strength of materials. Roy Swedish Inst Eng Res 1939:1–45.
[10] Weibull W. A statistical distribution function of wide applicability. J Appl Mech 1951;18:293–8.
[11] Bažant ZP, Xi Y, Reid SG. Statistical size effect in quasi-brittle structures: Part I is Weibull theory applicable? J Eng Mech 1991;117(11):2609–22.
[12] Carpinteri A. Scaling laws and renormalization groups for strength and toughness of disordered materials. Int J Solids Struct 1994;31:291–302.
[13] Herrmann HJ, Hansen A, Roux S. Fracture of disordered elastic lattices in two dimensions. Phys Rev B 1989;39(1):637–48.
[14] Alava MJ, Nukala PhKV, Zapperi S. Statistical models of fracture. Adv Phys 2006;55(3–4):349–476.

[15] Schlangen E, Van Mier JGM. Experimental and numerical analysis of the micromechanisms of fracture of cement-based composites. Cem Concr Compos 1992;14(2):105–18.
[16] Lilliu G, Van Mier JGM. 3D lattice type fracture model for concrete. Eng Fract Mech 2003;70(7/8):927–42.
[17] Prado EP, Van Mier JGM. Effect of particle structure on mode I fracture process in concrete. Eng Fract Mech 2003;70(14):793–1807.
[18] Van Mier JGM, Van Vliet MRA. Influence of microstructure of concrete on size/scale effects in tensile fracture. Eng Fract Mech 2003;70(16):2281–306.
[19] Joseph C, Jefferson AD. Stochastic regularisation of lattice modelling for the failure of quasi-brittle materials. In: Carpinteri A, Gambarova P, Ferro G, Plizarri G, editors. Proceedings FraMCoS-6 (fracture mechanics of concrete and concrete structures). London: Taylor & Francis Group; 2007. p. 445–52.
[20] Bolander JE, Shiraishi T, Isogawa Y. An adaptive procedure for fracture simulation in extensive lattice networks. Eng Fract Mech 1996;54:325–34.
[21] Man H-K, Van Mier JGM. Analysis of 2D- and 3D fracture scaling by means of 3D lattice simulations. In: Gdoutos EE, editor. Proceedings ECF-16 'fracture of nano and engineering materials and structures'. CD-ROM. Springer Publishers; 2006. p. 1–6.
[22] Man H-K, Van Mier JGM. Size and shape effects of fracture strength of concrete. In: Carpinteri A, Gambarova P, Ferro G, Plizarri G, editors. Proceedings FraMCoS-6 (fracture mechanics of concrete and concrete structures). London: Taylor & Francis Group; 2007. p. 39–44.
[23] Man H-K, Van Mier JGM. Influence of particle density on 3D size effects in the fracture of (numerical) concrete. Mech Mater 2007;40(6):470–86.
[24] Van Mier JGM. Multi-scale interaction potentials (F–r) for describing fracture of brittle disordered materials like cement and concrete. Int J Fract 2007;143(1):41–78.
[25] Emery JM, Hochhalter JD, Ingraffea AR Computational fracture mechanics of concrete structures: a retrospective through multiple lenses. In: Carpinteri A, Gambarova P, Ferro G, Plizarri G, editors. Proceedings FraMCoS-6 (fracture mechanics of concrete and concrete structures). London: Taylor & Francis Group; 2007. p. 3–15.
[26] Jayatilaka ADeS, Trustrum K. Statistical approach to brittle fracture. J Mater Sci 1977;12:1426–30.
[27] Danzer R, Supancic P, Pascual J, Lube T. Fracture statistics of ceramics – Weibull statistics and deviations from Weibull statistics. Eng Fract Mech 2007;74:2919–32.
[28] Roux S, Guyon E. Mechanical percolation: a small beam lattice study. J Phys Lett 1985;46:L999–L1004.
[29] Herrmann HJ, Roux S. Statistical Models for the Fracture of Disordered Media. Amsterdam: North Holland; 1990.
[30] Hansen A, Hinrichsen EL, Roux S. Scale-invariant disorder in fracture and related breakdown phenomena. Phys Rev B 1991;43(1):665–78.
[31] Hrennikoff A. Solutions of problems of elasticity by the framework method. J Appl Mech 1941;12:169–75.
[32] Roelfstra PE, Sadouki H, Wittmann FH. Le béton numérique. Mater Struct (RILEM) 1985;18:327–35.
[33] Schlangen E. Experimental and numerical analysis of fracture processes in concrete. PhD thesis, Delft University of Technology; 1993.
[34] Vervuurt A. Interface fracture in concrete. PhD thesis, Delft University of Technology; 1997.
[35] Van Mier JGM, Van Vliet MRA, Wang TK. Fracture mechanisms in particle composites: statistical aspects in lattice type analysis. Mech Mater 2002;34:705–24.
[36] Cusatis G, Bažant ZP, Cedolin L. Confinement shear–lattice model for concrete damage in tension and compression. I. Theory. J Eng Mech (ASCE) 2003;129(12):1439–48.
[37] Cusatis G, Bažant ZP, Cedolin L. Confinement shear–lattice model for concrete damage in tension and compression. II. Computation and validation. J Eng Mech (ASCE) 2003;129(12):1449–58.
[38] Ince R, Arslan A, Karihaloo BL. Lattice modeling of size effect in concrete strength. Eng Fract Mech 2003;70(16):2307–20.
[39] Wang J, Huet C. A numerical model for studying the influence of pre-existing microcracks and granular character on the fracture of concrete materials and structures. In: Huet C, editor. Micromechanics of concrete and cementitious composites. Lausanne: Presses Polytechniques et Universitaires Romandes; 1993. p. 229–40.
[40] Cundall PA, Strack ODL. A discrete numerical model for granular assemblies. Geotechnique 1979;29:47–65.
[41] Vonk RA. Softening of concrete loaded in compression. PhD thesis, Eindhoven University of Technology; 1992.
[42] Topin V, Delenne J-Y, Radjaï F, Brendel L, Mabille F. Strength and failure of cemented granular matter. Eur Phys J E 2007;23:413–29.
[43] Lilliu G. 3D-analysis of fracture processes in concrete. PhD thesis, Delft University of Technology; 2007.
[44] Man H-K. Analysis of 3D scale and size effects in numerical concrete. PhD thesis, ETH Zurich; 2009.
[45] Häfner S, Eckhardt S, Luther T, Könke. Mesoscale modeling of concrete: geometry and numerics. Compos Struct 2006;84:450–61.
[46] Van Vliet MRA. Size effect in tensile fracture of concrete and rock. PhD thesis, Delft University of Technology; 2000.
[47] Schlangen E. Computational aspects of fracture simulations with lattice models. In: Wittmann FH, editor. Proceedings FraMCoS-2 'fracture mechanics of concrete structures'. Freiburg: AEDIFICATIO Publishers; 1995. p. 913–28.
[48] Vořechovský M, Eliáš J. Mesh dependency and related aspects of lattice models. In: Oh BH, Choi OC, Chung L, editors. Evanston (IL): IA-FraMCoS; 2010 [CD-ROM].
[49] Rosset A, Spadola L, Ratib O. OsiriX: an open-source software for navigating in multidimensional DICOM images. J Digital Imaging 2004;17(3):205–16.
[50] Meyer D, Man H-K, Van Mier JGM. Fracture of foamed cementitious materials: a combined experimental and numerical study. In: Zhao H, Fleck NA, editors. In: Proceedings IUTAM symp 'mechanical properties of cellular materials'. IUTAM book series, vol. 12. Springer Science + Business Media; 2009. p. 115–23.
[51] Simioni S, Tschenett T. Investigation on the size effect on strength of concrete with realistic aggregate shapes. BSc thesis, Institute for Building Materials, Department of Civil, Environmental and Geodetic Engineering, ETH Zurich; 2007.
[52] Man H-K, Van Mier JGM. Size effect on strength and fracture energy for numerical concrete with realistic aggregate shapes. Int J Fract 2008;154:61–72.
[53] Eliáš J, Frantík P, Vořechovský M. Improved sequentially linear solution procedure. Eng Fract Mech 2010;77:2263–76.
[54] Lingen EJ. Design of an object-oriented finite element package for parallel computers. PhD thesis, Delft University of Technology; 2000.
[55] Bažant ZP, Oh O-H. Crack band theory for fracture of concrete. Mater Struct (RILEM) 1983;16(93):155–77.
[56] Zech B, Wittmann FH. A complex study on the reliability assessment of the containment of a PWR, Part II probalistic approach to describe the behaviour of materials. Nucl Eng Des 1978;48:563–93.
[57] Van Vliet MRA, Van Mier JGM. Experimental investigation of size effect in concrete and sandstone under uniaxial tension. Eng Fract Mech 2000;65(2/3):165–88.
[58] Van Mier JGM. Reality behind fictitious cracks? In: Li VC, Leung CKY, Willam KJ, Billington SL, editors. Proceedings FrAMCoS-5 'fracture of concrete and concrete structures'. Evanston (IL): IA-FraMCoS; 2004. p. 11–30.
[59] Van Mier JGM. Framework for a generalized four-stage fracture model of cement-based materials. Eng Fract Mech 2008;75:5072–86.
[60] Van Mier JGM. Mode I fracture of concrete: discontinuous crack growth and crack interface grain bridging. Cem Concr Res 1991;21(1):1–15.
[61] Trtik P, Stähli P, Landis EN, Stampanoni M, Van Mier JGM. Micro-tensile testing and 3D imaging of hydrated Portland cement. In: Carpinteri A, Gambarova P, Ferro G, Plizarri G, editors. Proceedings FraMCoS-6 (fracture mechanics of concrete and concrete structures). London: Taylor & Francis Group; 2007. p. 1277–82.
[62] Landis EN, Nagy EN. Three-dimensional work of fracture for mortar in compression. Eng Fract Mech 2000;65:223–34.
[63] Hillerborg A, Modeer M, Petersson P-E. Analysis of crack formation and crack growth in concrete by means of fracture mechanics and finite elements. Cem Concr Res 1976;6:773–82.